



Hierarchical Representation of Measurement Data, Metrological Uncertainty and Metadata for Calibrated Battery Tests

Amin Moradpour,^[a] Manuel Kasper,^[a] Manuel Moertelmaier,^[a] Nawfal Al-Zubaidi R-Smith,^[a] and Ferry Kienberger^{*[a]}

We present an interoperable hierarchical data representation for battery tests, leading to improved scalability of data transmission and enhanced data accessibility and comprehensibility for both human interpretation and machine processing. The hierarchical data format includes the raw trace electrical measurement data, the metrological calibration and uncertainty data, the metadata such as experimental settings, instruments and software versions, as well as post-processed data such as electrochemical model fit parameters. This data representation allows repetition of the battery test under the exact same conditions such that identical results are achieved within defined error bounds. This is in line with the general F. A. I. R.

data approach and provides repeatability and traceability in the battery value chain. As an application of the hierarchical data representation, we show the classification of cells as pass/fail being performed with quantitative confidence levels. We demonstrate the complete workflow of establishing the hierarchical data structure for electrochemical impedance spectroscopy (EIS), starting from metrological traceability of the calibration and uncertainty analysis towards the storage of the structured data as a single integrated file that preserves the hierarchical data format. The structured data file is provided in JSON format in the Zenodo repository, as well as the program scripts to generate and read the JSON EIS files.

Introduction

Data interoperability in the battery value chain is essential for tracking battery materials, production processes, and performance data, ensuring that data can flow efficiently between battery manufacturers, suppliers, and end-users.^[1] Thereby, the concept of the digital battery passport has gained substantial momentum in the automotive sector as a prospective solution, with initiatives being led by the Global Battery Alliance.^[2] Along the battery value chain, a series of tests are typically conducted in various process steps to evaluate the state of the battery and its components, such as the high-potential (HiPot) testing of the separator membrane during cell production, the evaluation of self-discharge measurements (SDM) of cells for quality control, or electrochemical impedance spectroscopy (EIS) of battery packs for fast state-of-health (SoH) evaluations and end-of-life monitoring. The various components and cell tests ensure the quality and performance of batteries throughout their lifecycle from the production to second-life applications. For example, the HiPot test can be applied for the early detection of separator defects in the battery production chain,

detecting electrical discharges in electrode-separator composites.^[3] SDM is a fast potentiostatic method for measuring self-discharge rates of batteries during cell formation to sort out defective cells based on a μA discharge rate measured within minutes by holding the cell voltage constant.^[4]

Another widely used battery test method in R&D and quality control is EIS, where the impedance of a device-under-test (DUT) such as a cell, module or pack is measured by analyzing the DUT response to an exciting sinusoidal current at various frequencies.^[5] The DUT's voltage is perturbed by the excitation signal causing a deviation from its open-circuit value, which is recorded at each frequency, probing the frequency dependence of electrochemical processes within the cell. Thereby, the contribution of individual components of the cell can be distinguished within the overall response. Figure 1 shows a block diagram of the EIS setup and the data flow. The excitation signal generation block comprises of a signal waveform generator and a power amplifier that provides the desired voltage or current amplitude to stimulate the DUT. The EIS equipment is connected to the DUT by a four-wire Kelvin connection that allows for separate sensing of the response voltage. The current and voltage signals are processed and digitized in the response signal acquisition block and streamed to a host computer where the data processing is performed. The connection geometry of mechanical fixtures can vary, for example when connection cables are placed slightly differently, which can introduce different current paths that lead to different impedance results (see Figure 1, current path 1 and path 2). Once the voltages and currents are measured at all frequencies, the frequency-dependent impedances are calculated in a data processing and analysis step. Additional steps,

[a] Dr. A. Moradpour, M. Kasper, Dr. M. Moertelmaier, Dr. N. A.-Z. R-Smith, Dr. F. Kienberger
Keysight Laboratories Linz,
Keysight Technologies Austria GmbH
Linz 4020, Austria
E-mail: ferry_kienberger@keysight.com

© 2023 The Authors. *Batteries & Supercaps* published by Wiley-VCH GmbH.
This is an open access article under the terms of the Creative Commons Attribution License, which permits use, distribution and reproduction in any medium, provided the original work is properly cited.

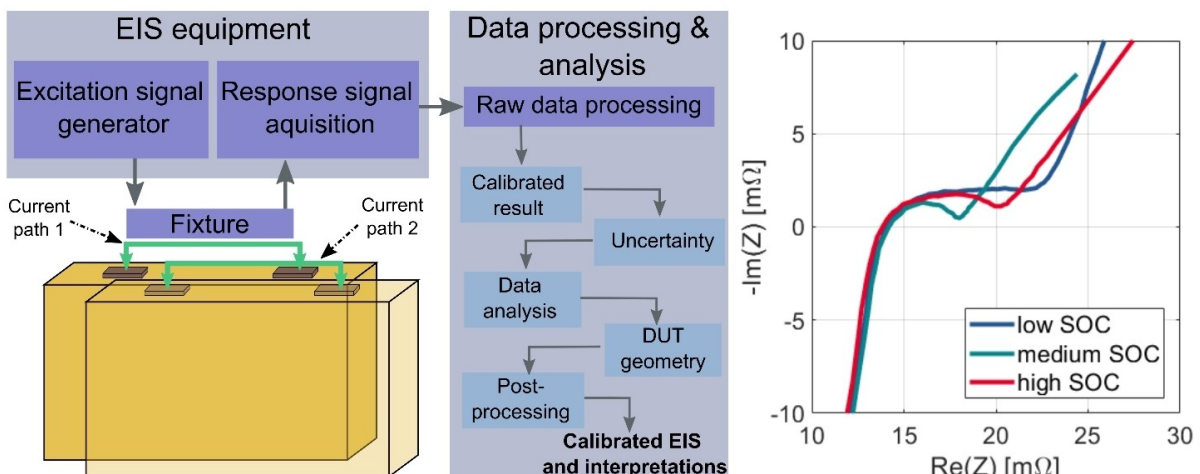


Figure 1. Measurement workflow for electrochemical impedance spectroscopy (EIS). The left panel shows the signal excitation, the mechanical fixture connecting to the cell, and the response signal acquisition using two different current paths. The middle panel shows the raw data processing and data analysis, including calibration, correction, and post-processing. The right panel shows calibrated EIS curves of a 40 Ah prismatic cell at three different SoCs resulting in different shapes which are further analyzed in the post-processing step to allow electrochemical interpretation.

such as impedance calibration and correction, are typically performed to convert the raw impedances to calibrated and corrected values. In a previous work,^[6] we developed a systematic three-error term calibration procedure that removes systematic errors during the measurement process. In addition, the measurements are also affected by random errors, leading to uncertainty in the measurement results.^[7] In a subsequent work,^[8] we therefore identified the source of random errors that influence the EIS results, providing a complete uncertainty analysis of the full EIS frequency range. All uncertainty sources, such as measurement noise and fixture repeatability, are characterized at different frequency points by measuring specific shunt standards in the given fixture geometry. The effects of the various uncertainty sources are then obtained on the final impedances by applying the uncertainty propagation to the three-term calibration procedure. Finally, in order to fully contextualize a measurement, further information is recorded as metadata. This includes user-provided information about measurement and post-processing software, geographical location of the experiments, the type of hardware used for experiments, or the physical geometry such as form and dimensions of the DUT. By employing a common data and metadata exchange format, the need for format conversions is minimized, leading to improved scalability.^[9] This is particularly crucial in a scenarios with multiple participants, such as the representants in the broad battery value chain, ranging from battery manufacturing to testing and recycling. Furthermore, emphasizing the consistent impedance values with defined error bounds at specific frequencies when testing the same battery cell with different hardware and fixtures enhances the repeatability across various system configurations and the accuracy of interlaboratory comparisons.^[6] Such replicability of battery test methods like EIS is essential, for example, in the electric vehicle (EV) industry, as it supports consistent and comparable results by incorporating detailed metadata and interoperable data formats, contributing for example to the

reliability of battery SoH assessments.^[10] Figure 1 shows the complete measurement and data processing workflow, from raw data acquisition to calibration and post-processing. In the post-processing step, electrochemical models are fit to the EIS curves in order to determine electrochemical properties like internal cell solution resistance and effective capacitances of the various interfaces.^[11] Typically, EIS measurements are highly dependent on SoC and temperature,^[12] which are also saved in the meta-data. Figure 1, right panel, shows the dependence of EIS on the state-of-charge (SoC) of a 40 Ah prismatic cell in a Nyquist plot, where a significant change of the width of the semi-circle is obtained at different SoCs.

Methods

EIS calibration and uncertainty workflow

Figure 2 shows the workflow to integrate EIS raw data, calibrated data, and the measurement uncertainty in a hierarchical data format. The left panel shows the EIS calibration, where error coefficients are obtained by employing calibration standards to perform calibration measurements. The error coefficients and the raw data are fed to the correction function to get the corrected results. The corrected EIS results are transferred to the structured data file (middle panel). The right panel represents the uncertainty propagation. The effects of uncertainty sources are included in the EIS results by considering them during calibration standard measurements and cell measurements. The uncertainties are propagated through the calibration and correction functions to obtain the calibrated results and their uncertainties at each single frequency point. A detailed description of the three-error term calibration and the metrological uncertainty analysis can be found in.^[6,8]

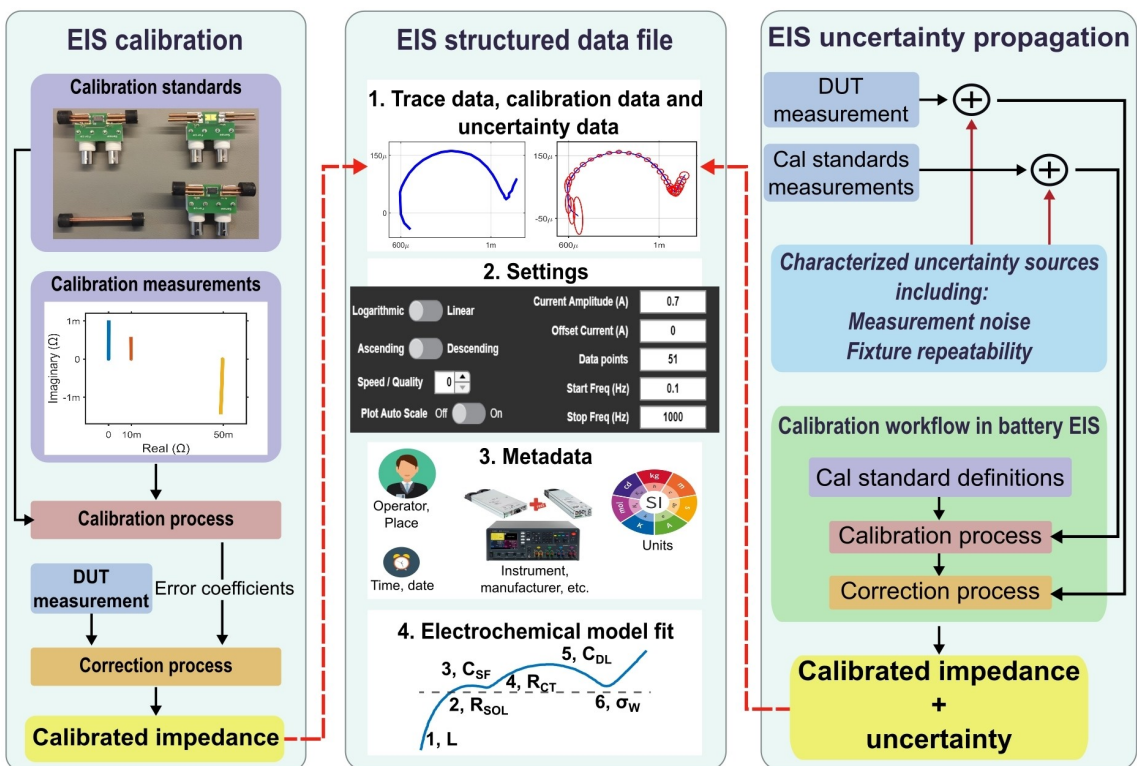


Figure 2. Calibration and uncertainty integration in the hierarchical data structure for EIS. The left panel shows the calibration and correction workflow. The right panel shows the uncertainty characterization. The middle panel shows the hierarchical data file where all the trace data, calibrated data, uncertainty, measurement settings, metadata, and post-processed data are integrated into one single data structure.

Results and Discussion

Battery test-data acquisition workflow

Figure 3 outlines the battery test data acquisition workflow and how data is aggregated into the structured battery test data format. The battery test can include a variety of different techniques to test either a single cell, a module or a full battery pack consisting of thousands of individual cells. Typical test methods include EIS, self-discharge measurements (SDM),^[4] charge and discharge cycles, or tests of battery sub-components like the high-voltage test of the separator membrane

(HiPot)^[3] (Figure 3, left box). These tests produce raw data in various formats. For example, in EIS, the signal source generates a sinusoidal current and applies it to the DUT through force cables, and the test hardware records the voltage response (Figure 3, left panel). The recorded currents and voltages are then transferred to the raw data processing block to calculate the impedance at specific frequencies (Figure 3, middle panel). Typically, in battery tests, the raw data is calibrated and corrected, and the uncertainty of the measurement is determined for each measurement point. The calibrated results and their uncertainties are then transferred to the data integration and file export block. For the complete battery test data set,

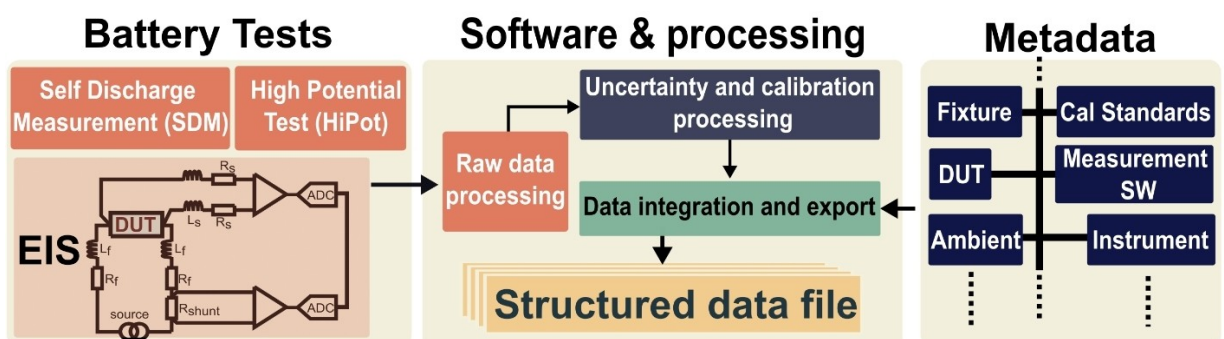


Figure 3. Battery test data and meta-data acquisition workflow. Left: Different techniques can be used to test a battery, including EIS, SDM, or HiPot. Middle: The response signal is passed to the raw data processing block, including correction of systematic errors and assigning measurement uncertainty. The raw and calibrated data, uncertainty data, and metadata are integrated into a hierarchical format and exported as a single file. Right: The measurement settings and different metadata are collected from the user.

additional data entered by the user is recorded, for example, metadata such as measurement settings, geographical location, details of fixtures used for the test, or instrument specifications (Figure 3, right panel). In the data integration block, all data is arranged in a hierarchical structure which can then be stored as a single integrated file, for example, in JSON or HDF5 format that support the hierarchical data arrangement.

The hierarchical data format structure

Figure 4 shows the proposed hierarchical data structure for general battery tests, covering for example EIS, SDM, HiPot, or charge-discharge cycling. The first-level block is labeled ‘Measurement’ and contains raw data and measurement settings. The second level ‘Data’ block combines different battery test results performed on a DUT, such as trace signals, post-processed signals, and calibrated quantities. In the third-level field ‘Settings’, each measurement is determined by multiple identifications (IDs) of the specific experiments, for example, the hardware and software versions, ambient conditions, and the type of DUT. Also, the conditions for the specific measurements are included such as start and stop frequency for EIS, number of points, and sweeping type. An additional first-level block is ‘Metadata’ with further information on the battery test. It is divided into several subgroups, for example, the ‘Ambient’ field including information on the test ambient conditions like humidity and temperature. Other fields in the metadata include the DUT description (e.g., ‘Cell’, ‘Module’, ‘Pack’), ‘Calibration’, ‘Fixture’ and ‘Standards’. Each metadata sub-level is labeled with an ID, which is used in the measurement block under the field ‘Dependencies’ to address specific metadata. For example, various instruments can be identified in the field ‘Metadata’ with different IDs, and the proper ID can be selected in the ‘Measurement/Data/Dependencies/Instrument’ field to retrieve the correct information about the instrumentation used for the

specific experiment. Some fields in the hierarchical data structure contain multiple layers in which multiple instances of that field exist (see Figure 4). Each instance is uniquely identified with an individual ID. For example, multiple instruments with varying specifications and functions may be used for a battery test, and by using multiple layers and instances, all measurement data and metadata can be consolidated into a unified file for a given DUT. This obviates the need for separate files in response to modifications in a single metadata component.

Use case of the hierarchical data structure

Figure 5 shows an example of how the information in the hierarchical data structure leads to an improved cell classification where good cells are separated from bad cells in an in-line EIS test of a 40 Ah prismatic cell. In a typical test lab, the operator puts the prismatic cell into a standardized mechanical fixture (Figure 5, upper left). Random mechanical movements of the cables and small deviations of the exact mechanical and electrical fixture geometry can lead to slightly different electrical current loops with different inductances that can affect the EIS measurements (Figure 5, lower left). With the extended battery test file, the effect of inductances can be corrected using the information from the fixture and battery position data, and removing the variances in the inductances in the post-processing stage. To adequately address the fixture-DUT position and geometry, the reference position is defined as the center of the positive pole (Figure 5, lower left), and various cell positions are measured with respect to the reference position. Additional to the raw-data EIS measurements, the calibrated and corrected results are stored in the data file as well as the uncertainty of the measurement. From the uncertainty field in the structured data file, the uncertainty bounds can be assigned to the various EIS frequency points and

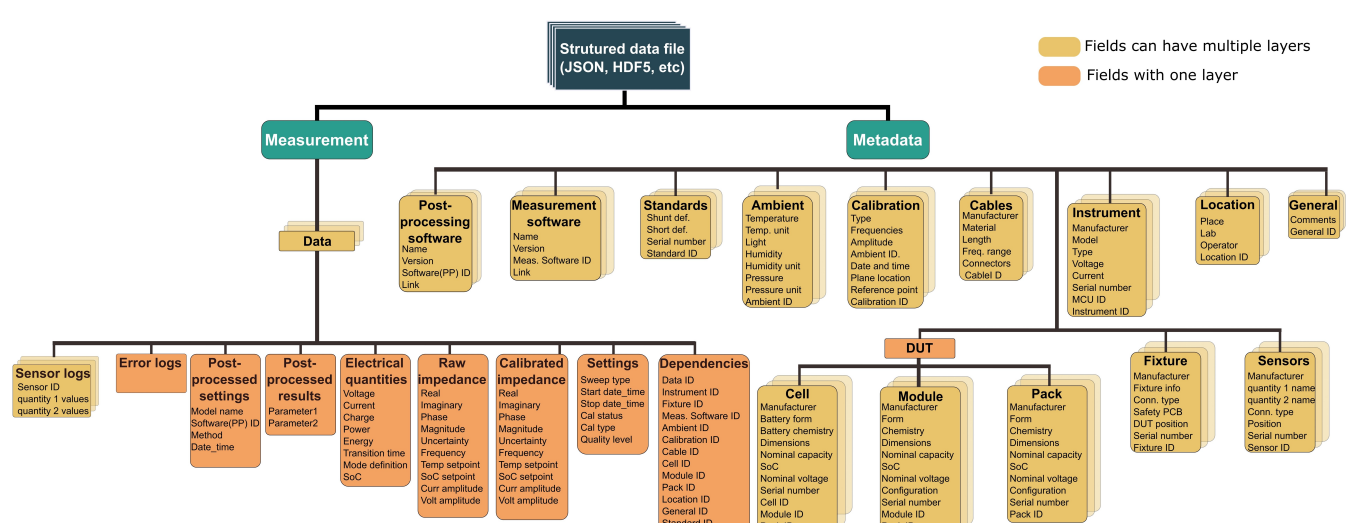


Figure 4. The hierarchical data structure for general battery tests. The structure has two main blocks, the ‘Measurement’ block and the ‘Metadata’ block. The data sources for the various subfields (brown boxes) are the measurement instrumentation, the user input data, and the post-processed data. The final data set can be exported in a single file such as JSON or HDF5.

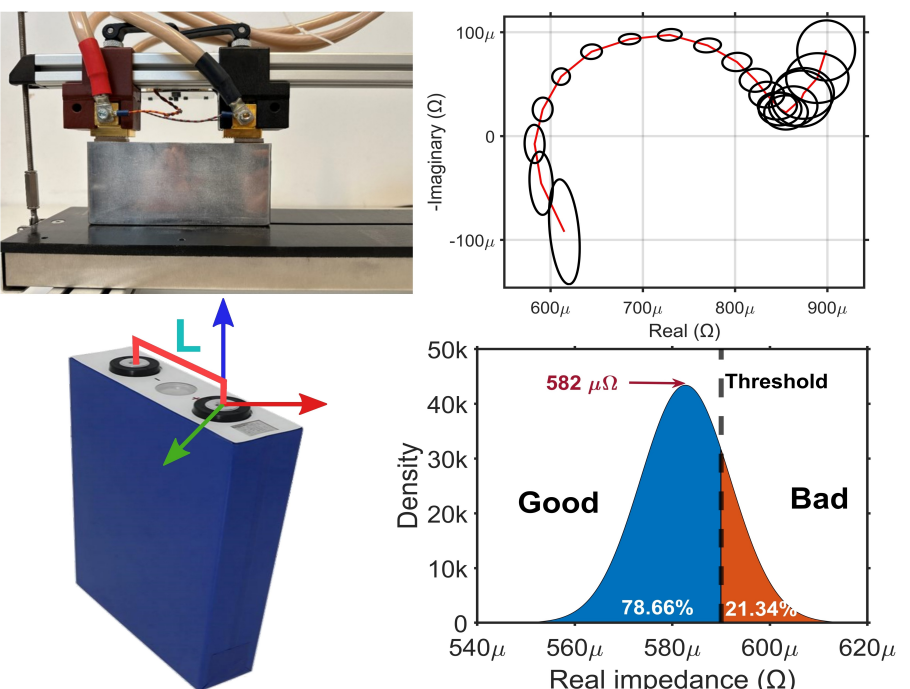


Figure 5. Application of the hierarchical data set for improved cell classification. Upper left: The placement of a 40 Ah prismatic cell in the mechanical fixture for EIS measurements. Lower left: Reference positions for the fixture-cell geometry relevant for error corrections of inductances L. Upper right: Nyquist plot of the EIS spectra of the 40 Ah prismatic cell with uncertainty bounds and confidence levels of 50%. Lower right: Probability density function (pdf) with the calibrated mean value of $582 \mu\Omega \pm 9.2 \mu\Omega$. The arbitrarily selected threshold of $590 \mu\Omega$ is indicated as dashed line, leading to the classification of the cell into good with 78.66% confidence level.

plotted in the Nyquist plot (Figure 5, upper right). The uncertainty error bounds and the calibrated EIS data are leading to an improved cell classification by providing a statistical confidence level (Figure 5, lower right). For this 40 Ah prismatic cell, the calibrated mean value and standard deviation is $582 \mu\Omega \pm 9.2 \mu\Omega$. The probability density function (pdf) with respect to the real part of the impedance is shown at a single frequency point assuming a Gaussian distribution of the uncertainties. Based on the arbitrary classification threshold that is provided by the user-input (here $590 \mu\Omega$; dashed vertical line), a quantitative confidence level (CL) can be assigned for the classification into a good or bad cell. While the calibrated mean value ($582 \mu\Omega$) is below the threshold ($590 \mu\Omega$), a simple binary classification without uncertainty levels would lead to a classification into a good cell. However, taking into account the uncertainty and the statistical test, the classification results in a CL of only 78.66% to be a good cell, and 21.34% being a bad cell.

Conclusions

The hierarchical data format presented in this paper contains recorded raw data, post-processed data (e.g., calibrated data, uncertainty, electrochemical fit parameters), and metadata (e.g., mechanical fixture information, environmental conditions, user-specific comments, hardware version). Thereby, a standardized data set is provided that is based on metrological measurements which are repeatable and traceable. The data set

includes the relevant data to adequately describe the battery test, allowing to repeat the test under the exact same conditions such that the same results are received within defined error bounds. This is in line with the general F. A. I. R. data approach^[13] and provides repeatability and traceability in the battery value chain.

We demonstrate the complete workflow of establishing the hierarchical data structure for EIS, where the raw impedances are fed to calibration and uncertainty processing in order to correct the systematic errors and to include the uncertainty data for each measured frequency point. The structured data file extends its utility beyond EIS, providing an adaptive and organized format for different types of battery tests. For instance, time-series data of the battery SDM can be easily organized, facilitating the identification of anomalies in the self-discharge behavior. In addition, for HiPot tests, the structured data format facilitates the systematic analysis of failure events in the battery cell separator membrane.

Table 1 gives an overview of how the data structure supports these various battery test methods. While EIS experiments require the most variety of data fields, other tests like HiPot, SDM, or charge-discharge cycling have less extensive requirements, and some fields of the hierarchical data format are either not filled or optional. For example, the field 'Standards' is only required for EIS but not for the other tests. Similarly, calibration is not required for HiPot and cycling, while it is required for EIS and SDM.

The use of hierarchical data structures allows for improved data tracing and interoperability between different users over

Data Structure	
	Metadata
Measurement	Cal Standards Alerts Cables Instruments Location Fixture Sensors DUT Calibration
Post-processing	Software Script Post-processing
Settings	Raw Calibration Interpretation Cables Raw Interpretation Electrical Quantities Settings Log(Telem) Settings Post-processed Sensor
Eros	SDM HPD Cycling SDM EIS

■ Data field required ■ Data field not required ■ Data field optional.

Table 1. The overall data field requirements for various battery tests including EIS, SDM, HPD, and cell cycling.

the entire battery value chain, including battery production sites, test labs, electric vehicles manufacturers, and 2nd life applications (Figure 6). Figure 6, left panel, shows a battery ecosystem that has evolved organically over time and features a multitude of producers and consumers of data, with data exchange happening through many point-to-point connections. With multiple parties involved that each create and consume data, the amount of necessary format conversions is expected to grow quadratically, even if not all possible pairs of senders and receivers exist. This makes adding new participants in the battery value chain challenging. With a large enough number of participants, it therefore becomes advantageous to enforce a common exchange format for data and metadata resulting in a star-shaped topology (Figure 6, right panel). In such a setting, the number of format conversions grows only linearly as new participants are added, resulting in improved scalability. A file format like JSON (JavaScript Object Notation) naturally allows the export of the hierarchical data structure while preserving its organizing tree. This is more efficient than flattening the data structure into tabular or linear text format. JSON stands thereby as an efficient low sized data interchange format that is widely employed to structure and facilitate data transmission across a spectrum of scenarios, such as between a server and a web application or among distinct components within a software ecosystem.^[15] The hierarchical EIS data shown in this paper is provided in the Zenodo repository as a JSON file. The JSON file format is encompassing data representation, data exchange, data import and export, configuration and customization, as well as the handling of metadata and annotations. Furthermore, it is common practice to enrich ontologies with additional contextual information related to concepts and relationships. In future work, the hierarchical data structures presented in this paper will be mapped to ontologies like the EMMO (Elementary Multiperspective Material Ontology) in order to establish a common language and framework for materials science and engineering. In the context of energy storage materials and devices, the use of standardized ontologies and the proposed battery data structure will allow for improved human interpretation and machine processing in the broad battery value chain.^[14]

Acknowledgements

This work was partially funded by the European Union Horizon 2020 project NanoMECommons (Grant Agreement no. 952869) and the project BatteryLife (project no. Wi-2022-603642) an FTI Initiative Kreislaufwirtschaft from the Upper Austrian Government.

Conflict of Interests

The authors declare no conflict of interest.

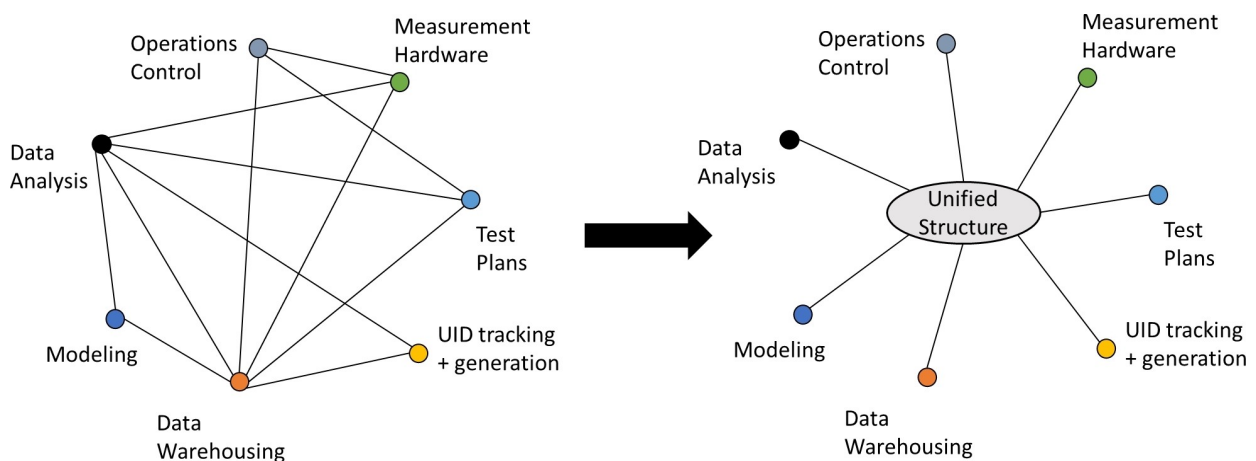


Figure 6. Improved interoperability across the battery value chain. Left: The required number of exchange protocols and format conversions is expected to grow quadratically with the number of participants even in a network that is not fully connected. Right: A unified data and metadata exchange format can serve as a central hub in this network, resulting in a linear growth of connections.

Data Availability Statement

The data supporting this research are openly available under the MIT license agreement in the Zenodo repository at <https://zenodo.org/uploads/10245135> under the identifier 10.5281/zenodo.10245135. The entry includes also the program scripts to generate and read the hierarchical data files in JSON format.

Keywords: battery test · calibration and uncertainty · data structure · electrochemical impedance spectroscopy (EIS) · interoperability · metadata standards

- [1] a) J. Wessel, A. Turetskyy, O. Wojahn, T. Abraham, C. Herrmann, *Procedia CIRP* **2021**, *104*, 1215–1220; b) L. Ward, S. Babinec, E. J. Dufek, D. A. Howey, V. Viswanathan, M. Aykol, D. A. C. Beck, B. Blaiszik, B.-R. Chen, G. Crabtree, V. de Angelis, P. Dechent, M. Dubarry, E. E. Eggleton, D. P. Finegan, I. Foster, C. Gopal, P. Herring, V. W. Hu, N. H. Paulson, Y. Preger, D. U. Sauer, K. Smith, S. Snyder, S. Sripad, T. R. Tanim, L. Teo, *Joule* **2021**, *6*, 19; c) G. dos Reis, C. Strange, M. Yadav, S. Li, *Energy and AI* **2021**, *5*, 100081; d) S. Clark, F. L. Bleken, S. Stier, E. Flores, C. W. Andersen, M. Marcinek, A. Szczesna-Chrzan, M. Gaberscek, M. R. Palacin, M. Uhrin, J. Friis, *Adv. Energy Mater.* **2022**, *12*, 2102702; e) E. Ayerbe, M. Berecibar, S. Clark, A. A. Franco, J. Ruhland, *Adv. Energy Mater.* **2022**, *12*, 2102696.
- [2] Global Battery Alliance Battery Passport, Global Battery, [Online]. Available: <https://www.globalbattery.org/media/pilot/documents/gba-bp-pilot-master.pdf> [Accessed September 2023].
- [3] L. Hoffmann, M. Kasper, M. Kahn, G. Gramse, G. Ventura Silva, C. Herrmann, M. Kurrat, F. Kienberger, *Batteries* **2021**, *7*, 64.
- [4] N. Al-Zubaidi R-Smith, G. Gramse, M. Moertelmaier, M. Kasper, F. Kienberger, in *2020 IEEE International Instrumentation and Measurement Technology Conference (I2MTC)* **2020**, pp. 1–5.
- [5] a) P. Vadiva, J. Hu, M. J. Johnson, R. Stocker, M. Braglia, D. J. L. Brett, A. J. E. Rettie, *ChemElectroChem* **2021**, *8*, 1930–1947; b) A. Moradpour, M. Kasper, F. Kienberger, *Batteries & Supercaps* **2023**, *6*, e202200524; c) A. Lasia, in *Modern Aspects of Electrochemistry* (Eds.: B. E. Conway, J. O. M. Bockris, R. E. White) Springer US, Boston, MA, **2002**, pp. 143–248; d) N. Al-Zubaidi R-Smith, M. Leitner, I. Alic, D. Toth, M. Kasper, M. Romio, Y. Surace, M. Jahn, F. Kienberger, A. Ebner, G. Gramse, *J. Power Sources* **2021**, *512*, 230459.
- [6] M. Kasper, A. Leike, J. Thielmann, C. Winkler, N. Al-Zubaidi R-Smith, F. Kienberger, *J. Power Sources* **2022**, *536*, 231407.
- [7] a) S. Han, Z. Meng, O. Omisore, T. Akinyemi, Y. Yan, *Micromachines* **2020**, *11*, 1021; b) M. Asprou, E. Kyriakides, M. M. Albu, *IEEE Trans. Instrum. Meas.* **2019**, *68*, 2808–2818.
- [8] A. Moradpour, M. Kasper, J. Hoffmann, F. Kienberger, *IEEE Trans. Instrum. Meas.* **2022**, *71*, 1–9.
- [9] I. E. Castelli, D. J. Arismendi-Arrieta, A. Bhowmik, I. Cekic-Laskovic, S. Clark, R. Dominko, E. Flores, J. Flowers, K. Ulvskov Frederiksen, J. Friis, A. Grimaud, K. V. Hansen, L. J. Hardwick, K. Hermansson, L. Koeniger, H. Lauritzen, F. Le Cras, H. Li, S. Lyonnard, H. Lorrmann, N. Marzari, L. Niedzicki, G. Pizzi, F. Rahamanian, H. Stein, M. Uhrin, W. Wenzel, M. Winter, C. Wölke, T. Vegge, *Batteries & Supercaps* **2021**, *4*, 1803–1812.
- [10] A. Temporelli, M. L. Carvalho, P. Girardi, *Energy* **2020**, *13*, 2864.
- [11] a) N. Meddings, M. Heinrich, F. Overney, J.-S. Lee, V. Ruiz, E. Napolitano, S. Seitz, G. Hinds, R. Raccichini, M. Gaberscek, J. Park, *J. Power Sources* **2020**, *480*, 228742; b) S. Buteau, J. R. Dahn, *J. Electrochem. Soc.* **2019**, *166*, A1611.
- [12] Q. Zhang, C. G. Huang, H. Li, G. Feng, W. Peng, *IEEE Transactions on Transportation Electrification* **2022**, *8*, 4633–4645.
- [13] M. D. Wilkinson, M. Dumontier, I. J. Aalbersberg, G. Appleton, M. Axton, A. Baak, N. Blomberg, J.-W. Boiten, L. B. da Silva Santos, P. E. Bourne, J. Bouwman, A. J. Brookes, T. Clark, M. Crossas, I. Dillo, O. Dumon, S. Edmunds, C. T. Evelo, R. Finkers, A. Gonzalez-Beltran, A. J. G. Gray, P. Groth, C. Goble, J. S. Grethe, J. Heringa, P. A. C. 't Hoen, R. Hooft, T. Kuhn, R. Kok, J. Kok, S. J. Lusher, M. E. Martone, A. Mons, A. L. Packer, B. Persson, P. Rocca-Serra, M. Roos, R. van Schaik, S.-A. Sansone, E. Schultes, T. Sengstag, T. Slater, G. Strawn, M. A. Swertz, M. Thompson, J. van der Lei, E. van Mulligen, J. Velterop, A. Waagmeester, P. Wittenburg, K. Wolstencroft, J. Zhao, B. Mons, *Sci. Data* **2016**, *3*, 160018.
- [14] M. Schreiner, A. Bhowmik, T. Vegge, J. Busk, O. Winther, *Sci. Data* **2022**, *9*, 779.
- [15] V. Ryen, A. Soylu, D. Roman, *Future Internet* **2022**, *14*, 129.

Manuscript received: November 2, 2023

Revised manuscript received: December 11, 2023

Accepted manuscript online: December 13, 2023

Version of record online: December 21, 2023